JOURNAL OF MATERIALS SCIENCE 20 (1985) 1015–1026

Fatigue crack growth in plate specimens under Mode III loading

W. J. PLUMBRIDGE
Department of Mechanical Engineering, University of Bristol, University Walk, Bristol, UK

Fatigue crack growth in plate specimens of aluminium and an aluminium alloy has been investigated under Mode III loading conditions. It has been found that only when a fully plastic situation exists, does crack extension proceed by a valid Mode III mechanism. When plasticity is restricted to planes of maximum shear there is a strong component of Mode I cracking which results in delamination in the direction of macroscopic growth. Under constant load amplitude cycling the crack growth curve exhibits three stages: a reduction in rate is followed by a period of steady growth prior to acceleration in the final stages. Such a profile is independent of material condition or failure mechanism. Cycling between fixed displacement limits leads to a reducing growth and crack arrest which occurs at a length proportional to the square of the displacement.

1. Introduction

There exist three fundamental modes by which crack extension can occur. In the Opening Mode (Mode I), the crack surfaces move directly apart; in the Edge-Sliding Mode (Mode II), the crack surfaces slide over each other perpendicular to the leading edge of the crack; and in the Tearing Mode (Mode III), the crack surfaces slide with respect to each other parallel to the leading edge. For conditions within the domain of linear elastic fracture mechanics the crack tip situation may be described by the appropriate stress intensity term (K_I, K_{II} or K_{III}). When crack propagation under cyclic loading is considered, a good empirical agreement is found between the growth rate da/dN and the Mode I stress intensity range, for a substantial proportion of the life of long cracks, i.e.

$$\frac{da}{dN} = C(\Delta K_I)^m$$

where C and m are constants. In situations where plasticity dominates, the equivalent ΔJ or COD terms replace ΔK. In practice, cracks commonly grow under mixed, rather than single, mode conditions and Mode III components occur during crack penetration in torsion (Mode II + Mode III), and in tensile loading of sheet or plate specimens following the onset of "slant-growth" (Mode I + Mode III).

Few data are also available for Mode II conditions [1–5] but only recently has there been any substantial experimental assessment of crack growth in a Mode III situation [6–9]. These have generally involved cyclic torsion of notched cylinders and have been based on the assumption of uniform concentric growth inwards. In pure torsion fracture surface interaction occurs at low stress levels (or with limited amounts of plasticity), which reduces the effective crack tip stress intensity and also makes reproducible measurement difficult. Such interaction is a result of a "factory roof" fracture surface profile which is still capable of meshing with the opposing crack face and carrying load. Reliable measurements and a unique relationship between growth rate and ΔK_{III} are achieved if a small axial load is applied, which when its Mode I component is less than the Mode I threshold, does not affect the Mode III growth rate. As a consequence, reported comparisons between crack growth rates at nominally similar stress intensity levels in the two modes [8, 9] should be examined with care. From endurance tests on notched cylinders it has been suggested that the threshold for

0022–2461/85 $03.00 + .12

crack growth Mode III exceeds that for Mode I [10].

The present paper reports the findings of an investigation into crack growth under cyclic Mode III loading in plate specimens, with particular emphasis on material condition and the induced failure mechanisms.

2. Experimental details

2.1. Straining frame

The general layout of the rig, together with the final specimen geometry, is shown in Fig. 1 and is described in detail elsewhere [11]. Cyclic displacements were achieved using a variable crank (up to ± 30 mm), driven by a geared d.c. motor, the speed of which could be controlled via its variable armature resistance. A lever arm (3:1) was employed in the system to reduce the load on the motor arm and to enable increased sensitivity in load adjustment. The specimen, a flat plate containing side grooves (see below), was supported at its sides by blocks, through which an in-plane transverse force could be applied if required. The central portion of the plate, bounded by the grooves, was displaced out-of-plane relative to the fixed end sections by a connecting rod in the loading line (Fig. 1b). A load cell was located adjacent to the specimen, and the displacement at the point of application of the load was measured using a linear variable differential transducer. The

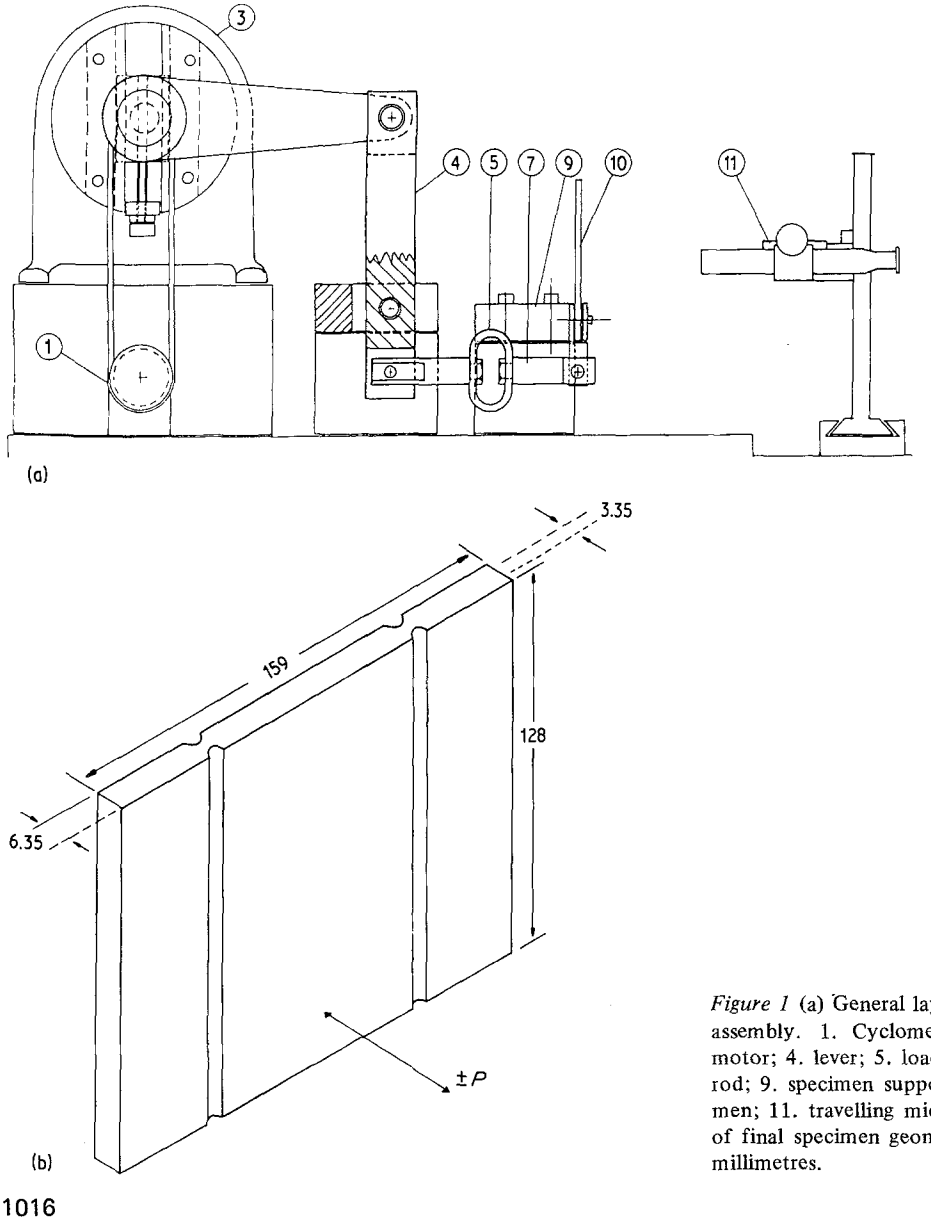

Figure 1 (a) General layout of the straining assembly. 1. Cyclometer; 3. geared d.c. motor; 4. lever; 5. load cell; 7. connecting rod; 9. specimen support blocks; 10. specimen; 11. travelling microscope. (b) Sketch of final specimen geometry. Dimensions in millimetres.

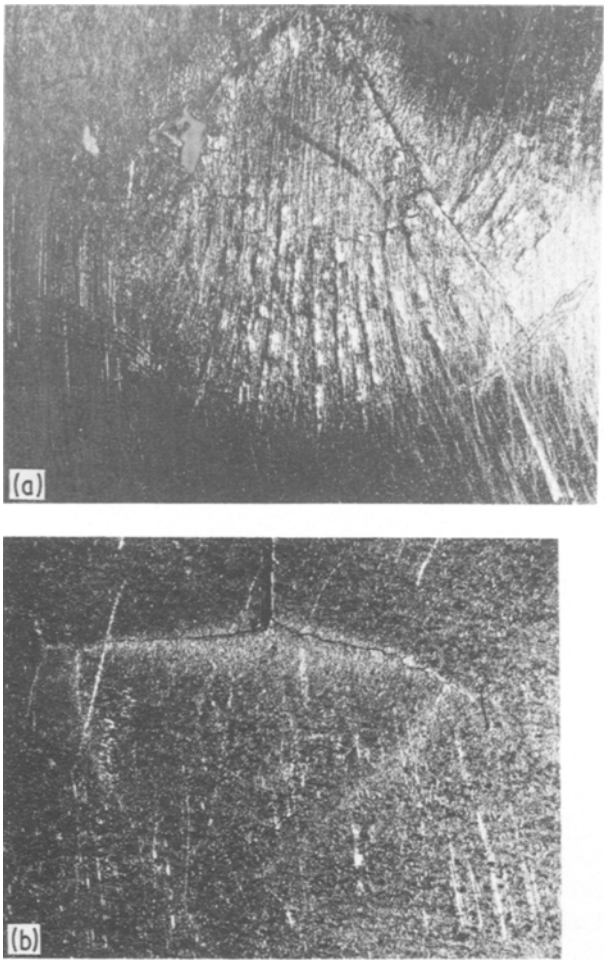

Figure 2 Crack branching in flat sheet specimens. (a) Aluminium, cyclic displacement ± 0.2 mm. (b) Mild steel, cyclic displacement ± 0.28 mm (× 1.5 approx.).

output of each was continuously monitored throughout every test. Changes in crack length were determined by a travelling microscope.

2.2. Specimen profile development

It had initially been intended that the specimen should consist simply of a flat plate containing two sawcuts to act as crack-starters. With this geometry, however, it was found that two cracks initiated from each notch, and between them existed an orthogonal network of minor cracks (Fig. 2). The included angle of the fan of damage increased as the displacement amplitude was raised. For aluminium it was approximately 45° at ± 0.2 mm and 80° at ± 0.3 mm whilst in mild steel it was 170° at ± 0.28 mm. By using the grooved profile shown (Fig. 1b), this effect could be eliminated and the growth of a single crack along the base of the groove was achieved. Notches were inserted using a jeweller's saw, with a razor blade to sharpen the tip. To improve microscopic detection of the crack tip the surface of each groove root was polished longitudinally to a 1 μm finish. With this geometry, bending of the plate was detectable only when the crack length exceeded 40 mm. It was estimated at about 10% at a crack length of 60 mm (i.e. at the completion of most tests).

2.3. Materials and testing procedure

Plates of a cold-rolled commercially pure aluminium, and an aluminium alloy, in both its as-quenched and fully aged conditions, were examined. Tests were carried out either at constant displacement amplitudes or at "constant" load ranges. In the latter case a load decrease of 5% was permitted before adjusting the eccentricity of the crank to restore the load to original value; this decrease was caused by the change in compliance due to the propagation of the crack.

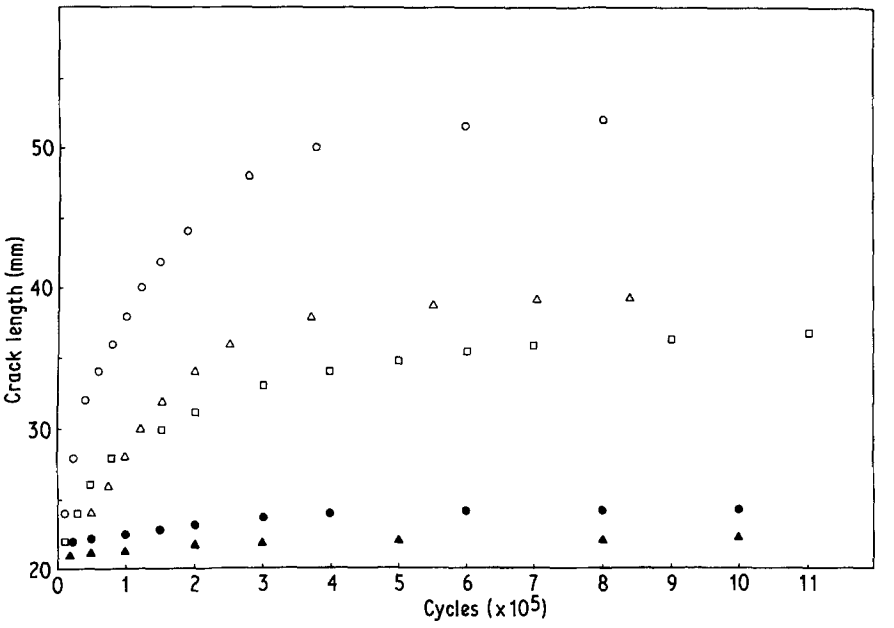

Figure 3 Crack growth in aluminium under displacement control. ○ ± 0.50 mm; △ ± 0.38 mm; □ ± 0.36 mm; ● ± 0.23 mm; ▲ ± 0.20 mm.

3. Results

3.1. Crack growth during constant displacement cycling

Each specimen of the pure metal and the as-quenched alloy contained two cracks (one in each groove), and an average value of the crack length is reported since the coincidence between individual lengths was good (within 5%). Length measurements quoted are actual crack growth from the notch tip.

With a fixed displacement amplitude at the plate edge the tearing moment at the crack tip diminishes as the crack grows. This produces an initially high propagation rate which falls continuously until the cessation of growth (Fig. 3). As would be expected, the greater the displacement amplitude, the longer the final crack. The associated changes in load again demonstrate a reduction in tearing force as the crack grows (Fig. 4). At the highest displacements this fall is substantial (≃ 40%), but its magnitude diminishes for small displacements until there is virtually no change at ± 0.1 mm. A direct quantitative comparison between the various tests cannot be made since it is not possible to reproduce exactly the dimensions of the starter notch, and additionally, the extent of cyclic hardening or softening ahead of the crack tip will vary according to the local strain amplitude.

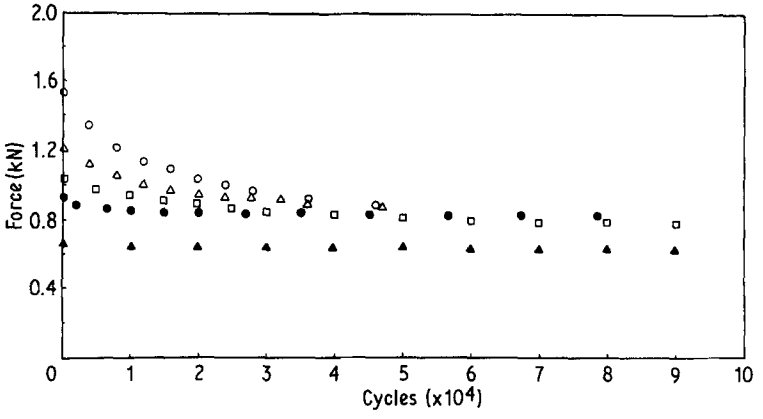

Figure 4 Force changes during displacement-controlled cycling of aluminium. ○ ± 0.50 mm; △ ± 0.38 mm; □ ± 0.36 mm; ● ± 0.23 mm; ▲ ± 0.20 mm.

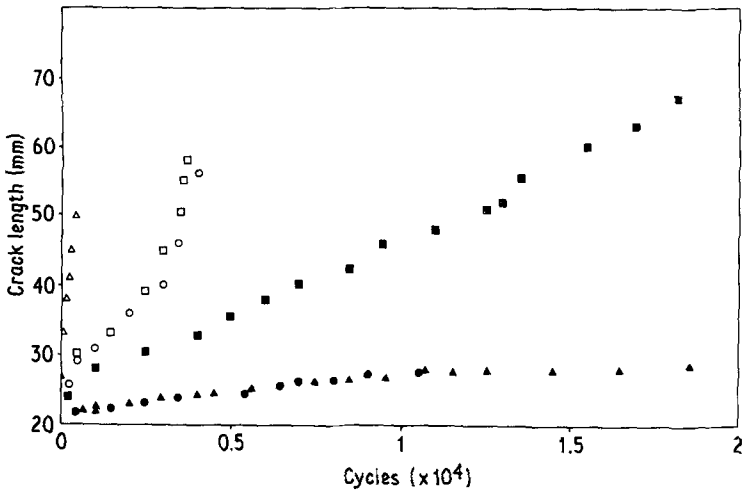

Figure 5 Crack growth in fully aged aluminium alloy under load control. △ ± 1.5 kN; □ ± 1.0 kN; ○ ± 0.9 kN; ■ ± 0.75 kN; ●, ▲ ± 0.5 kN.

3.2. Crack growth under "constant" load range cycling

Load adjustments had to be made numerous times during each test to maintain constancy of load amplitude as the fatigue crack propagated, but these produced no detectable effect on the growth curve. In the fully aged alloy specimen two parallel cracks grew along each groove equally offset from its base. They were of similar length and an average value was assumed.

As with constant displacement cycling, crack growth is initially rapid, but the rate of propagation attains a fairly constant level before increasing again near final failure (Figs. 5 and 6). The duration of the period of steady growth diminishes as the load amplitude increases, whilst at the lowest load range examined it is not apparent whether growth will eventually cease or accelerate to failure. These features apply to the alloy in both its fully aged and as-quenched conditions and also to the impure aluminium. The effect of material and heat treatment is shown in Fig. 7, in which the smallest endurance is exhibited by pure aluminium. The as-quenched alloy has a similar "steady state" growth rate to that of the aged condition but acceleration occurs earlier to give a shorter life.

3.3. Fractography of Mode III

The details of the optical fractography are presented in Table I. For the fully heat-treated alloy cycled under load control, longitudinal fracture surface undulations and channelling in the direction of crack growth develop into a vertical delamination of the specimen (Figs. 8a and b). This splitting tended to occur at greater crack lengths

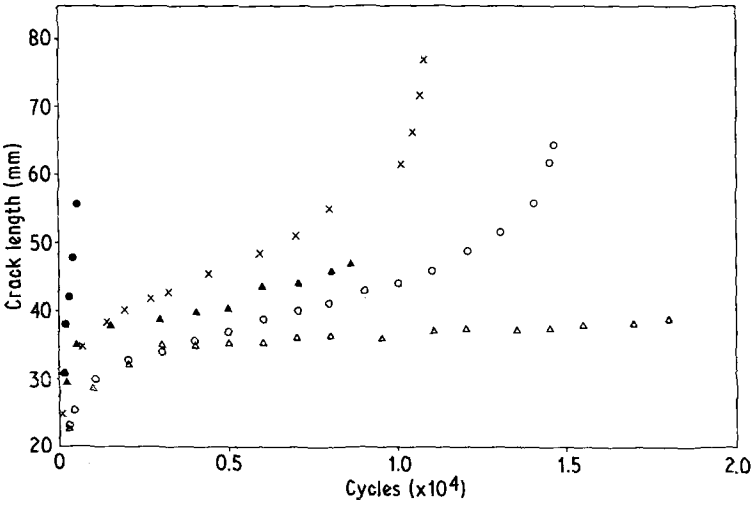

Figure 6 Crack growth in the as-quenched alloy and the pure aluminium under load control. X ± 0.75 kN (Al); ● ± 1.0 kN; ▲ ± 0.85 kN; ○ ± 0.75 kN; △ ± 0.5 kN (alloy).

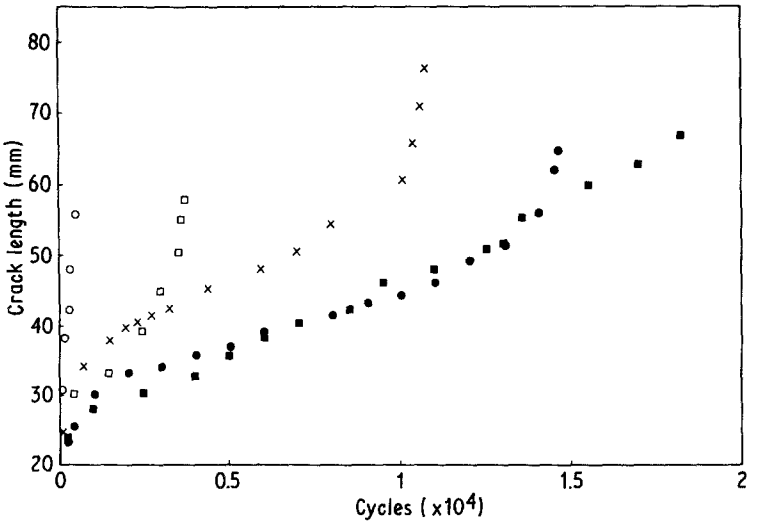

Figure 7 Crack growth curves showing effect of material and heat treatment under load control. ■ ± 0.75 kN; □ ± 1.0 kN (alloy – aged). ● ± 0.75 kN; ○ ± 1.0 kN (alloy – as-quenched). X ± 0.75 kN (pure aluminium).

for higher load. Evidence for macroscopic rubbing or sliding was also apparent, with the latter more visible at the lower loads. In the quenched condition no delamination occurred. On almost all surfaces it was replaced by through-the-thickness transverse grooving which tended to develop a concave curvature at long crack lengths (Figs. 9a and b). Dark areas covered with fretting product were most noticeable at lower load levels, but became less evident at long crack lengths. The pure aluminium exhibited similar features to the as-quenched alloy under both load and displacement cycling.

At higher magnifications it can be seen that the channelling and delamination apparent on the fracture surface of the fully aged alloy is a consequence of secondary cracking on planes perpendicular to the macroscopic crack surface and the thickness dimension, i.e. in the plane of the plate (Fig. 10). In those regions where they are not rubbed smooth the uppermost peaks which constitute the channels appear to fail by ductile tearing (Figs. 10a, b, c). On the fracture surfaces of the as-quenched alloy and the pure metal most features are obliterated by the attrition between the crack faces, with the exception in some areas of shallow circular voids (Fig. 11). Application of a small side tensile load during cycling reduces contact between the crack faces and reveals secondary cracking along width shear planes perpendicular to the growth direction (Fig. 12). To complete the fractographic survey a specimen was loaded monotonically in Mode III to failure and examined.

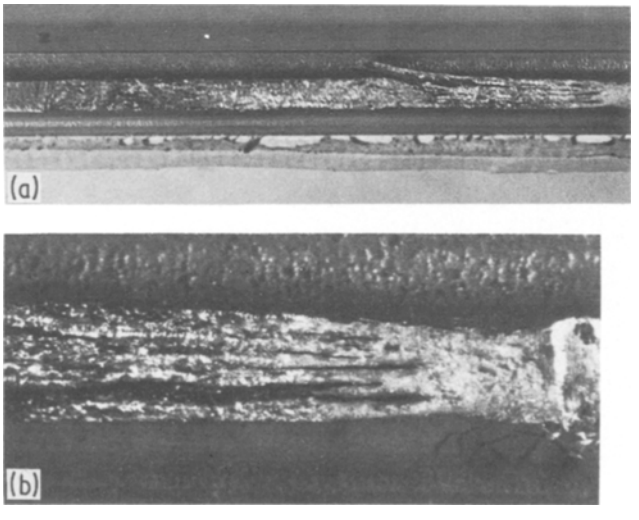

Figure 8 Optical fractography of fully aged alloys showing delamination effect. (a) Low magnification with starter notch on left-hand side and tensile fracture region on right-hand side (× 2). (b) Close-up of final region of crack growth (× 5.5).

TABLE I Summary of fractographic observations

Material/condition	Load range (kN)	Crack length (mm)	Features	Crack length (mm)	Features	ΔK_{III} at delamination (MPa $m^{1/2}$	Plastic zone size (mm)
Alloy/aged	± 1.5	20–54	Bright, channelling	54–64	Vertical delamination	19.4	1.78
Alloy/aged	± 1.0	20–45	Bright, channelling	45–55	Vertical delamination	11.8	0.66
Alloy/aged	± 0.75	20–26.5	Fretting + channelling	26.5–33	Slight vertical delamination	6.8	0.22
Alloy/aged	± 0.5	20–25	Copious fretting	25–33	Vertical delamination	4.4	0.09
Alloy/as-quenched	± 1.0	20–44	Coarse transverse rubbing, bright	44–55	Slight concavity of rub marks	–	–
Alloy/as-quenched	± 0.85	20–40	Coarse transverse rubbing, heavy fretting, bright	40–45	Undulations with little fretting	–	–
Alloy/as-quenched	± 0.75	20–46	Coarse transverse rubbing, heavy fretting, bright	46–66	Shallower rub marks with no fretting	–	–
Alloy/as-quenched	± 0.5	20–37	Coarse transverse rubbing, heavy fretting, bright	37–40	Concave front	–	–

Assuming LEFM conditions exist, $\Delta K_{III} = \tau(\pi a)^{1/2}$, $r_p = 1/\pi(\Delta K_{III}/2\tau_y)^2$ where τ_y is the shear yield stress, i.e. $\sigma_y/3^{1/2}$.

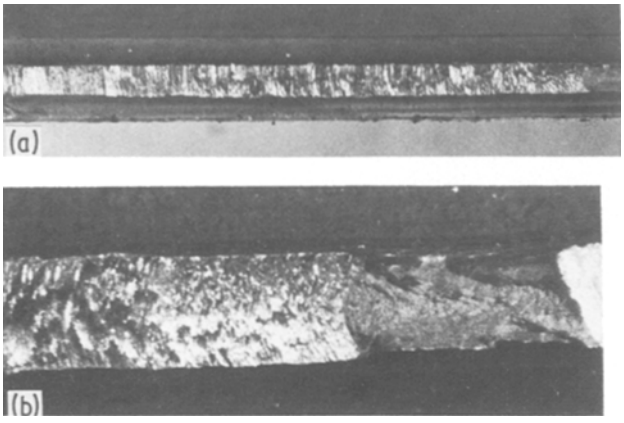

Figure 9 Optical fractography of the alloy in the as-quenched condition showing coarse transverse markings. (a) Starter notch left-hand side, tensile fracture right-hand side (× 2). (b) Close-up of crack and tensile fracture region (× 7).

The fracture surface exhibited heavily elongated ductile dimples (Fig. 13) in contrast to the equiaxed variety generally formed by tensile Mode I loading.

4. Discussion

The conditions in few of the tests reported in this work have fallen within the confines of linear elastic fracture mechanics. Only at the lowest loads in the aged alloy has the crack tip plastic zone remained small with respect to the specimen thickness, whilst in the as-quenched alloy and the pure metal the dimensions of the two are similar. In addition, because of the geometry of the specimen, it is unlikely that singularity conditions will apply, which precludes a stress intensity or a J integral correlation. The major findings in terms of the fractography and form of the crack growth curve are now considered.

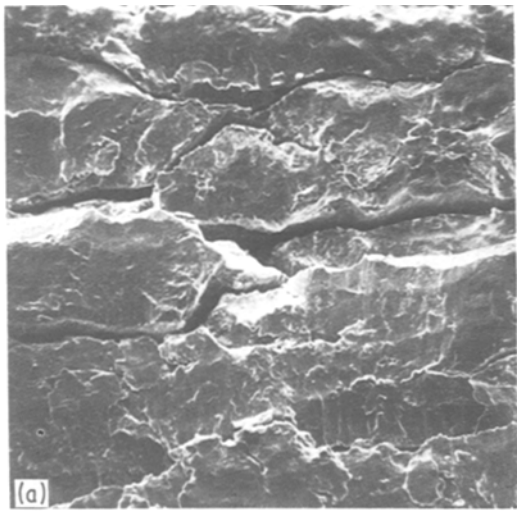

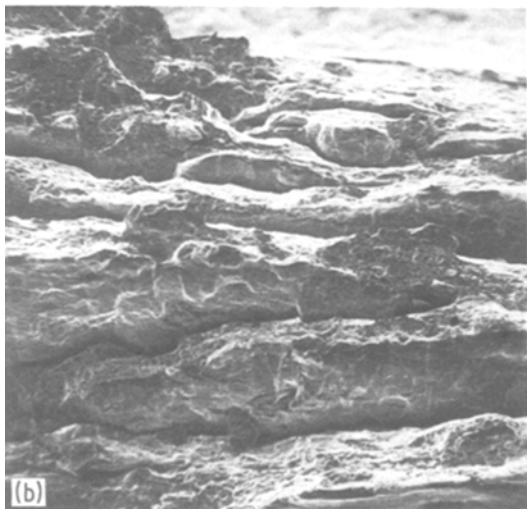

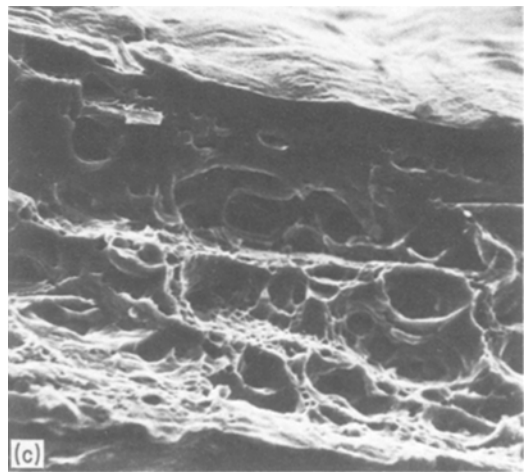

Figure 10 SEM fractographs of delamination regions in the fully aged alloy. (a) Peaks of channels smoothed by attrition (× 80). (b) Peaks undamaged showing evidence of ductile tensile failure (× 38). (c) as (b) × 800. Crack growth left to right.

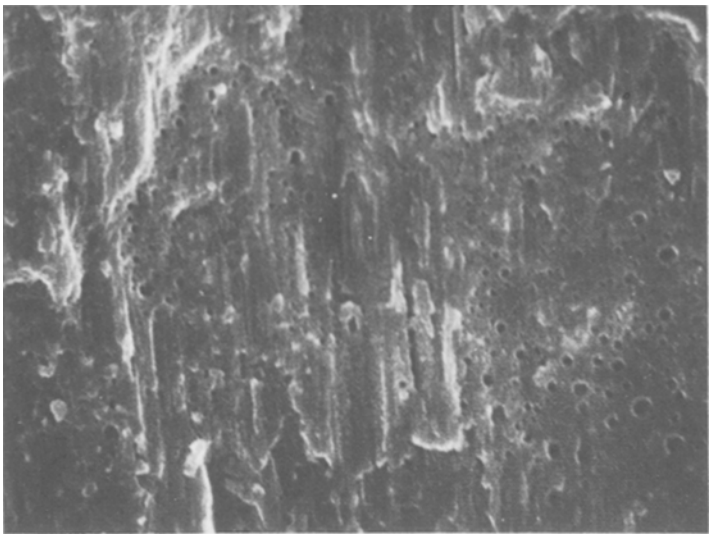

Figure 11 SEM fractograph of as-quenched alloy showing rub marks (× 2190).

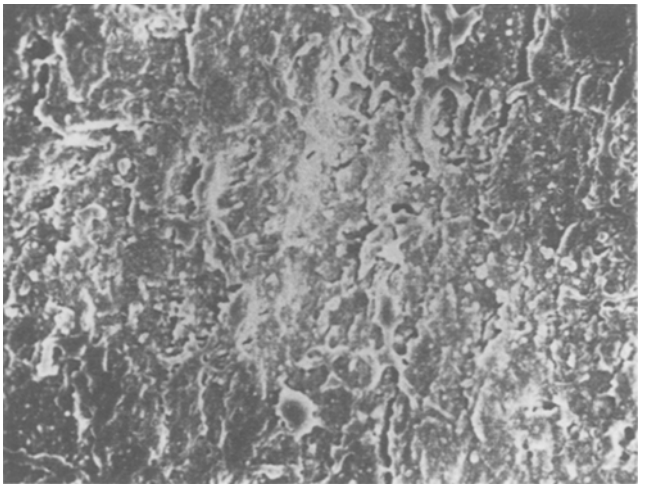

Figure 12 Secondary transverse cracking revealed in pure aluminium on the application of a small tensile side load (× 525).

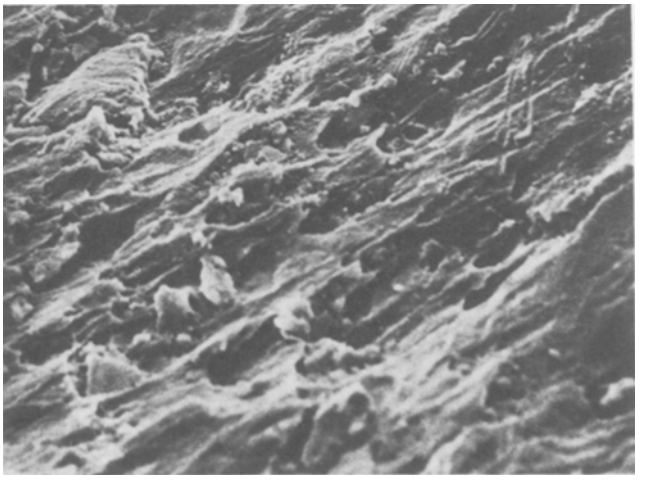

Figure 13 Monotonic failure caused by Mode III loading (× 750).

4.1. Fractographic observations

Two types of failure have been identified under Mode III loading according to the extent of crack tip plasticity. In the fully plastic situation, as in the as-quenched alloy and the pure metal, the crack faces move out-of-plane as evidenced by the regular through-thickness grooving (Fig. 9). This is akin to the classic mechanism for Mode III crack extension. Fretting also occurs, but to a diminishing extent as the crack tip extends and the crack faces are held further apart by an enlarged crack tip plastic zone [6]. At very long crack lengths a degree of concavity is observed in the grooving which is indicative of a Mode II component of growth. The appearance of these straight transverse grooves on the fracture surface supports the validity of Mode III loading even on a microscale, since localized bending would produce the curvature in the grooves which is observed only at the very longest crack lengths. When the degree of plasticity is small and restricted to the shear planes, as in the aged alloy, longitudinal channelling in the direction of crack growth and eventual delamination are visible (Fig. 8). These arise due to secondary cracking in Mode I (Fig. 14a). Sectioning through a crack demonstrates the multi-mode growth which also results in the double crack formation for the alloy in this condition (Fig. 14).

The crack length at which delamination is observed increases with increasing stress level but there appears to be no simple criterion for its onset. For example, assuming LEFM applied for all cases, Table I shows that the plastic zone size is not a constant at this transition.

4.2. Form of the crack growth curves

In this section the profiles of the plots of crack length, a, against the number of cycles, n, are considered. The profile produced during constant displacement cycling, revealing a gradual reduction in growth rate, is not unexpected since as the crack propagates the applied strain range at the crack tip diminishes. Under the conditions examined the crack length at its arrest is proportional to the square of the initial displacement. The growth curve resulting from constant load cycling, however, is unusual in that for most of the load ranges employed a three-stage process is revealed. Initially, the crack propagates rapidly but then slows to a fairly steady rate before accelerating towards failure. Early reductions in growth have been reported in the vicinity of notches in Mode I cycling [12–14], but in the present case the effect is apparent over substantially larger crack lengths which are broadly similar for the three conditions examined (Fig. 7). For Mode III growth induced by torsion of cylindrical bars, reductions in growth rate have also been reported [6], but since that test method restricts crack extension to a few millimetres, the presence of a minimum value and subsequent acceleration has

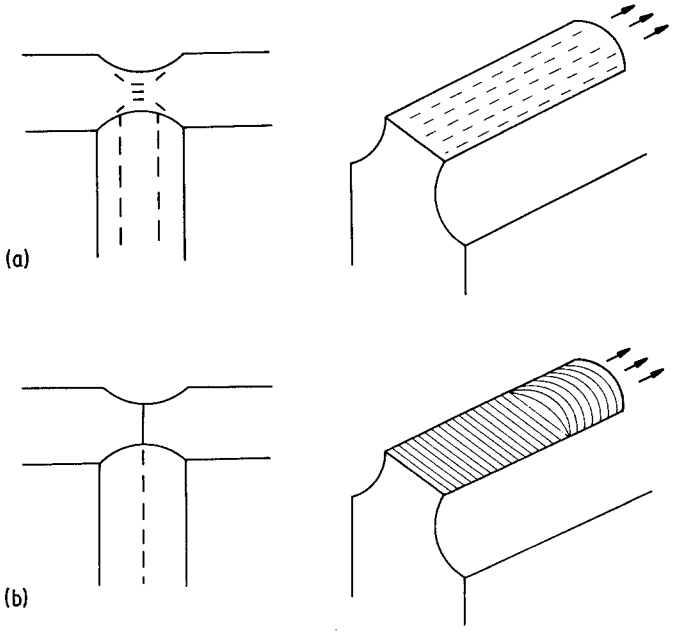

Figure 14 Schematic of types of crack growth under Mode III loading. (a) Limited plasticity and multiple cracking. (b) Gross plasticity, through-thickness grooving and a single crack.

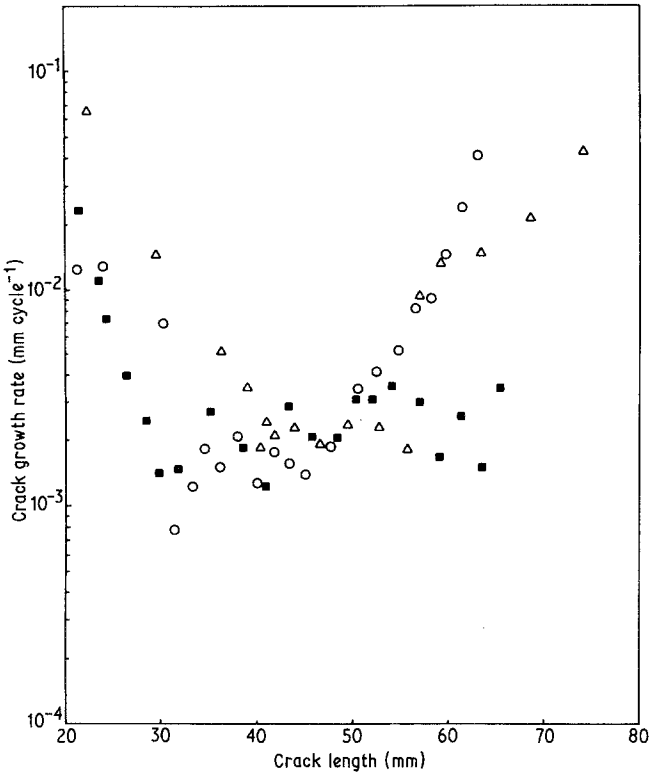

Figure 15 Crack growth rate as a function of crack length and material condition. Load range ± 0.75 kN. ■ Aged alloy; ○ as-quenched alloy; △ pure aluminium.

not been previously identified. Growth rate data equivalent to the a against n curves of Fig. 7 are presented in Fig. 15, which, together with Table II, demonstrates the sensitivity of the minimum growth rate to applied stress level and the small effect of material condition. With reducing loads the minimum in growth rate becomes smaller and is observed at shorter crack lenths in both alloy conditions. As previously mentioned, there is considerably more scatter in growth rates than normally encountered during Mode I fatigue.

With regard to the existence of any link between the profile of the crack growth curve and fracture surface appearance, it must be concluded that, for this specimen geometry, it is unlikely. For the aged condition the onset of delamination follows the same variation with applied load and crack length as does the minimum in the growth rate curve, but there is no direct quantitative correlation. It may be argued that delamination is the culmination of a gradual channelling along the direction of growth over most of the initial crack length. More important, however, is the fact that although the crack growth profiles are similar for all three conditions tested, delamination was observed only in the fully aged alloy. In the as-quenched alloy and the pure aluminium a totally different fracture surface topography is produced, suggesting a geometry/mechanics explanation for the form of the growth curves. This is supported by inspection of the LEFM solution for the variation of stress intensity with crack length in a edge-cracked rectangular bar under torsion [15, 16]. In this case K falls significantly during crack growth up to about $0.3W$, where W is the specimen width. Thereafter, it remains fairly constant until a $\simeq 0.7W$, when it increases slightly prior to approaching zero at very long crack lengths.

TABLE II Minimum growth rate data under load-control cycling

Material	Load (kN)	$(da/dN)_{min}$ (mm cycle^{-1})	Crack length (mm)
Alloy – aged	1.5	3.2×10^{-2}	40.5
	1.0	3.5×10^{-3}	31.0
	0.9	4.1×10^{-3}	30
	0.75	1.45×10^{-3}	30
	0.5	2×10^{-4}	26
Alloy – as-quenched	1.0	4×10^{-2}	50
	0.85	8×10^{-4}	38
	0.75	8×10^{-4}	32
	0.5	1.4×10^{-4}	36
Pure metal	0.75	1.9×10^{-3}	40.5

5. Conclusions

From experiments involving Mode III loading (or straining) of plate specimens it has been found that:

1. The Mode III crack extension is produced only when a fully plastic situation prevails. In this case, through-thickness grooving is the principal fractographic feature.

2. When plasticity is limited a Mode I component of growth arises which results in channelling and eventual delamination of the fracture surface in the macroscopic direction of growth.

3. Under constant load amplitude cycling the crack growth curve (a against n) generally exhibits three stages. The growth rate falls initially, then remains constant prior to increasing near final failure. This profile is independent of material or failure mechanism.

4. Under fixed displacement cycling the growth rate diminishes until crack arrest which occurs at a length proportional to the square of the displacement.

References

1. R. ROBERTS and J. KIBLER, *Trans. Amer. Soc. Mech. Eng.* **93** (1971) 671.
2. D. L. JONES and D. B. CHISHOLM, *Eng. Fracture Mech.* 7 (1975) 261.
3. L. P. POOK and A. F. GREENEN, Proceedings of the Conference on Fatigue Testing and Design (Society of Environmental Engineering, London, 1976) Paper 30.
4. A. OTSUKA, K. MORI, T. OHSHIMA and S. TSUYAMA, "Advances in Fracture Research" (Fifth International Conference on Fracture, Cannes, 1981) p. 1851.
5. G. HUA, M. W. BROWN and K. J. MILLER, *Fatigue Eng. Mater. Struct.* **5** (1982) 1.
6. E. K. TSCHEGG, *Mater. Sci. Eng.* **54** (1982) 127.
7. R. O. RITCHIE, F. A. McCLINTOCK, H. NAYEB-HASHEMI and M. A. RITTER, *Metall. Trans.* **13** (1982) 101.
8. E. K. TSCHEGG, R. O. RITCHIE and F. A. McCLINTOCK, *Int. J. Fatigue* **5** (1983) 29.
9. E. K. TSCHEGG, *J. Mater. Sci.* **18** (1983) 1604.
10. L. P. POOK and J. K. SHARPLES, *Int. J. Fracture* **15** (1979) 223.
11. W. R. ARSCOTT and M. E. DALSKI, University of Bristol, Department of Mechanical Engineering Report No. 76/B/1 (1976).
12. R. A. SMITH and K. J. MILLER, *Int. J. Mech. Sci.* **19** (1977) 11.
13. J. S. SANTER and M. E. FINE, *Metall. Trans.* 7 (1976) 583.
14. W. J. PLUMBRIDGE, *Metal Sci.* **12** (1978) 251.
15. R. A. WESTMAN and W. H. YANG, *J. Appl. Mech.* **34** (1967) 693.
16. D. P. ROOKE and D. J. CARTWRIGHT, "Compendium of Stress Intensity Factors" (HMSO, London, 1974) p. 253.

Received 29 March
and accepted 10 May 1984